High-throughput triggered merging of surfactant-stabilized droplet pairs using traveling surface acoustic waves

Vincent Bussiere, Aurélie Vigne, Andreas Link, John Mcgrath, Aparna Srivastav, Jean-Christophe Baret, Thomas Franke

High-throughput triggered merging of surfactant-stabilized droplet pairs using traveling surface acoustic waves

Vincent Bussiere[†Ψ], Aurélie Vigne[†‡Ψ], Andreas Link[†], John McGrath[†], Aparna Srivastav[†], Jean-Christophe Baret[‡+]*, Thomas Franke[†]*

[†]Biomedical Engineering, School of Engineering, University of Glasgow, Glasgow, G12 8LT, United Kingdom

[‡]Université de Bordeaux, CNRS, Centre de Recherche Paul Pascal, Unité Mixte de Recherche 5031, Pessac, 33600, France

[+]Institut Universitaire de France, 75005 Paris

*E-mail : jean-christophe.baret@u-bordeaux.fr
*E-mail : Thomas.Franke@glasgow.ac.uk

ABSTRACT: We present an acoustofluidic device for fluorescently triggered merging of surfactant-stabilized picoliter droplet pairs at high throughput. Droplets that exceed a preset fluorescence threshold level are selectively merged by a traveling surface acoustic wave (T-SAWs) pulse. We characterize the operation of our device by analyzing the merging efficiency as a function of acoustic pulse position, duration and acoustic pressure amplitude. We probe droplet merging at different droplet rates and find that efficient merging occurs above a critical acoustic power level. Our results indicate that the efficiency of acoustically induced merging of surfactant stabilized droplets is correlated with acoustic streaming velocity. Finally, we discuss how both time-averaged and instantaneous acoustic pressure fields can affect the integrity of surfactant layers. Our technique, by allowing the merging of up to 10^5 droplets per hour, shows a great potential for integration into microfluidic systems for high-throughput and high-content screening applications.

Droplet-based microfluidics enables the precise control and analysis of (bio)chemical reactions[1] and provides a powerful platform for high throughput single-cell screening in large cell populations.[2] Droplets play an essential role in numerous fields, including protein engineering,[3] oncology,[4] stem cells research[5], material sciences.[6], systems and synthetic biology.[7,8] They act as picolitre sample carriers that can be systematically sorted,[9] trapped,[10] mixed,[11] pipetted[12] and split[13] in a user-defined process to reproduce bench-top protocols at higher throughput and lower cost.

Merging is central to many droplet-based microfluidic systems since it triggers and starts chemical reactions. Droplet merging can be performed using passive or active techniques. Passive techniques are easily implementable in microfluidics as they rely on microfluidic channel designs which give rise to hydrodynamic forces that enable merging of drops in a non-selective, high-speed manner.[14] Active merging is generally preferred since it permits on-demand coalescence of selected surfactant-stabilized droplet pairs.[14–16] Surfactant molecules are used in droplet-based microfluidic systems because they significantly reduce the occurrence of non-specific coalescence by lowering emulsion interfacial tension to preserve sample compartmentalization.[17] In the widely used electro-coalescence, the droplet interface is destabilized by application of a high frequency and high voltage electric field.[19–21] Recently, a method using ferrofluid droplet pairs exposed to a uniform magnetic field was presented.[21] Yet, both strategies depend on the contrast between droplet and carrier fluid physicochemical properties, such as the conductivity, electrolyte concentration, pH-value or magnetic susceptibility, and are therefore limited in their scope of applications.[19–22] Another approach based on thermo-induced droplet merging can overcome this drawback. However, the need to use thermo-responsive microgels for droplet surface stabilization limits its applicability and temperatures required can potentially harm cells or denature proteins in samples.[22]

The use of travelling surface acoustic waves (T-SAWs) is a versatile alternative for merging. They provide a fast actuation mechanism for droplets[9,12,13,23] that can be triggered on-demand and which is independent of their physicochemical properties. Furthermore, surface acoustic waves are considered a biocompatible manipulation tool, and have been used with a variety of cells and biological samples.[24–26] So far, two methods using T-SAWs for the droplet merging have been reported. In the first, acoustic radiation forces immobilize droplets flowing through a channel expansion into a merging chamber.[27] Consecutive droplets are merged with the trapped droplet, modifying the drag force to acoustic radiation force ratio until a critical size is reached, leading to the release of the merged ensemble. This approach, inspired from passive merging, does not require droplet spacing adjustment. However, it involves the use of surfactant-free solutions, which increases the likelihood of unwanted coalescence events. To overcome this limitation, a second approach permitting the merging of surfactant stabilized droplets has been presented.[28] Easily implementable, the technique requires no special channel design and allows for the continuous droplet merging. Nonetheless, as T-SAW generation is not triggered and droplet content is not analyzed, the technology is restricted to unselective merging protocols.

In this article, we present a new acoustofluidic device that enables rapid, selective merging of individual droplet pairs, triggered by droplet fluorescence level. We characterize the acoustic droplet merger by analyzing the impact of critical operating parameters on merging efficiency and show that the main control parameters for merging droplet pairs are the pulse delay, power and duration.

MATERIALS & METHODS

Hybrid device fabrication. We use a tapered IDT (T-IDT) deposited on top of a piezoelectric substrate (polished, 128° rot, Y-cut LiNbO3), coated with a a 200 nm SiO_2 layer, to generate T-SAWs. The theoretical resonance frequency of the IDT ranges from 160 MHz to 167 MHz, allowing for sub-micrometer precision positioning of its 169 µm wide acoustic path along the aperture.[29]

Polydimethylsiloxane (PDMS) channels are made using standard soft lithography. The PDMS channels are manually aligned on the T-IDT chip with a precision of ± 10 µm, using a stereomicroscope. Both parts are then mechanically pressed against each other to create a seal before flushing channels with Aquapel to make them hydrophobic.

Fluidic system. For on-chip production of a binary emulsion, we use a double cross-junction module with all inlet widths set to 30 µm. 2% w/w FluoSurf (Emulseo, France) in 3M™ NOVEC™ 7500 fluorinated oil constitutes the continuous phase while deionized water (18,2 MΩ, MilliporeSigma) or deionized water with trypan blue and fluorescein (10 µM final) are used for the dispersed phases. The three inlets of the double cross-junction module are pressure-driven by the mean of a custom-made pressure pump system controlled in real-time on LabView (National Instruments). Typical working pressures range from 100-600 mbar, depending of the required droplet sizes and production frequencies. A programmable syringe pump (PHD ULTRA™, Harvard Apparatus) is employed to inject continuous phase for droplets spacing. Volumetric flows rates between 20 µl hr^{-1} and 200 µl hr^{-1} are used, depending on droplet frequencies.

Fluorescent signal detection and IDT actuation. To excite droplets, a 488 nm 200mW DPSS laser is aligned to the droplets' path. The fluorescence signal of individual droplets can be collected through a photomultiplier tube (H10723-20, Hamamatsu) before being analyzed in real-time by a custom-made LabView routine (LabView 2019, National instruments) complied on a field-programmable gate array (FPGA; NI PCIe 7841R, Virtex-5 LX30, 200kS.sec^{-1}, National instrument). If a droplet's fluorescence signal exceeds a user-defined threshold a delayed 5 V TTL signal is sent from the FPGA to trigger, with µsec precision, a switcher (ZX80-DR230-S+, Mini-Circuits) permanently fed with an HF signal coming from a signal generator (SMB 100A, Rohde & Schwarz). Next, the HF signal is redirected to the T-IDT and a T-SAW pulse is generated to merge the targeted droplet pair.

All experiments were performed on an inverted microscope (IX, 73) and recorded using a high-speed camera (Mini AX-50, Photron).

RESULTS

To achieve acoustic merging, we use a T-IDT composed of 60 finger pairs with finger spacing ranging from 23 µm to 24,3 µm along its 570 µm wide aperture, which generates T-SAW pulses on a piezoelectric $LiNbO_3$ substrate across an acoustic path width of 169 µm. The substrate is bound to a PDMS mold containing the microfluidic structures to enable the delivery of droplet pairs to the merging region of the chip.

We produce a mixture of two emulsions on-chip using a cross-junction channel. Through one side of the cross-junction an aqueous solution containing 10 µM fluorescein is dispersed, while the other side produces pure deionized water droplets. The continuous phase is made of fluorinated oil (HFE 7500, 3M™) containing 2% (w/w) FluoSurf™ (Emulseo, France). Droplets are produced in the squeezing regime at the junction and form a plug flow (Figure 1a). All three inlet channels composing the cross-junction have width W = 30 µm and height H = 25 µm. By modifying inlet driving pressures, the volumes and frequencies of each emulsion are adjusted independently. Control over droplet spacing is achieved by adding continuous oil phase to the emulsions (Figure 1b). The likelihood of unintended droplet splitting at the oil injector is reduced by the widening of its orifice to lower shear forces, while PDMS pillars prevent potential droplet expansion.

The droplets flow in an expanding channel section at the merging chamber entrance where fluorescence level is measured continuously using a laser-induced epifluorescence setup. The laser beam is focused upon the droplet and detects the fluorescence emission signal with a photomultiplier tube (Figure 1c). When the fluorescence level exceeds the threshold, a trigger actuates merging downstream. While flowing through the channel expansion, droplets with a diameter smaller than the maximum chamber width (W_{max} = 100 µm) become slower, allowing droplets that follow and span the channel width in plug-flow to catch up. This means that smaller droplets become the front drops of droplet pairs that will eventually merge, while the larger ones become the rear drops.

When the volumetric flow of the oil injector and the flow rate ratio between the two emulsions are adjusted, droplet pairs are precisely spaced such that only one pair arrives in the merging chamber at a time. Merging is induced by delivering an acoustic pulse, generated by a T-IDT, that hits the droplet pair as shown in Figure 1d. In the newly formed drop, aqueous solutions from both merged droplets mix quickly while the resulting drop exits the chamber (Figure 1e).

Exact timing and positioning of the acoustic pulse, with respect to the position of the droplets, is key to merging. When a drop exceeds the fluorescence threshold and the merging trigger is set, the acoustic pulse is delayed by a user-defined delay time D. By using this mechanism and selecting the appropriate operation frequency for T-IDT excitation, the time and location of the pulse is precisely controlled.

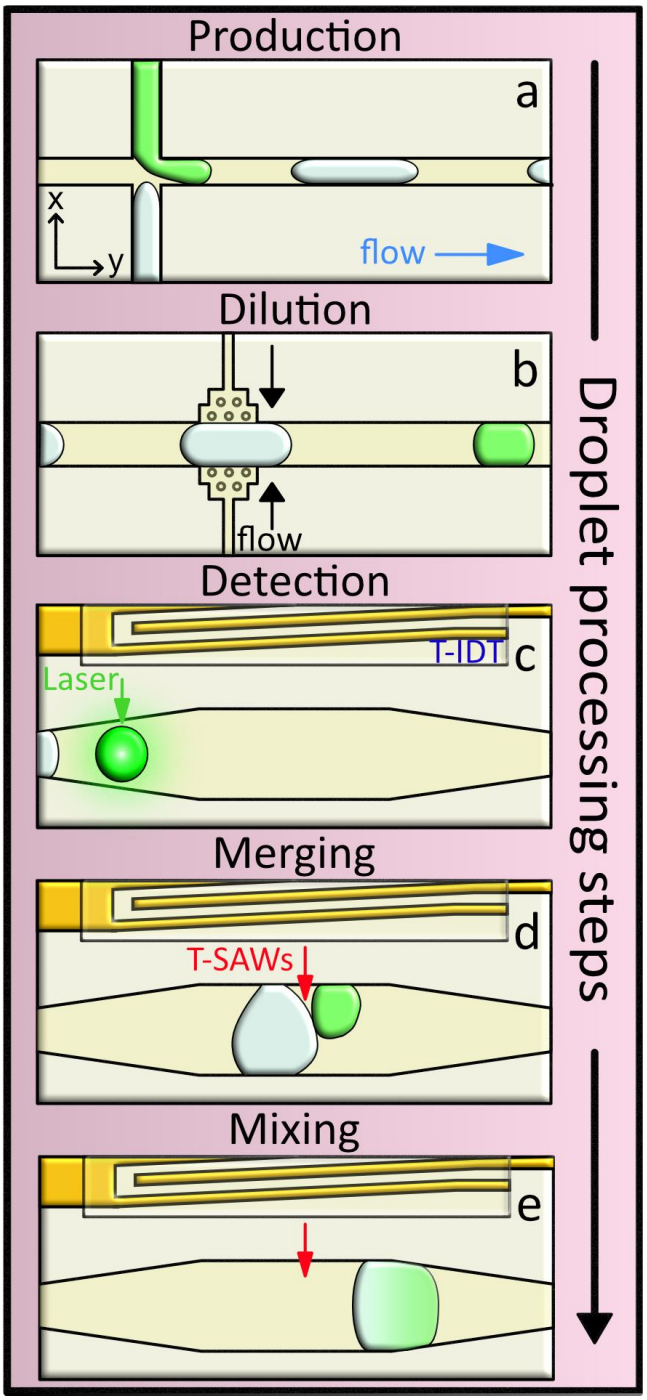

Figure 1. Schematic processing of droplets in the acoustic merging device. (a) Fluorescein (green) and water (blue) droplets of different diameters are synchronously produced in the squeezing regime forming droplet plugs. (b) Droplets are diluted by adding an oil phase from two sides. (c) Single drops' fluorescence level is screened at the merging chamber entrance and a trigger is set. (d) If the fluorescent signal of one drop exceeds a user-defined threshold, a T-SAW pulse is released and the droplet pair is merged. Blue, black green and red arrows depict the main channel flow, oil injection flow, the laser spot and T-SAWs pulse direction. Micrographs showing 1a and 1b are provided in *SI Appendix*, Figure S1.

An advantage of the presented merging device is its flexibility. By inverting the driving pressures of the two dispersed phases at the T-junction inlets, we can switch the position of the fluorescein droplets and the aqueous drops to trigger merging from front to back and vice versa, while still achieving successful merging (Figure 2a and 2b). If a fluorescein droplet is positioned in front of the pair to be merged, merging is considered as front-triggered (FT; Figure 2a). If the fluorescein droplet is at the rear of merged pair, merging is considered as back-triggered (BT; Figure 2b). Another advantage of a triggered system, is the ability to control the acoustic path location relative to the position of the targeted droplet pairs by adjusting the delay time, defined as $D = t_{TSAW} - t_{detect}$, where t_{TSAW} and t_{detect} are the times of T-SAW pulse generation and detection of a drop above the fluorescence detection threshold.

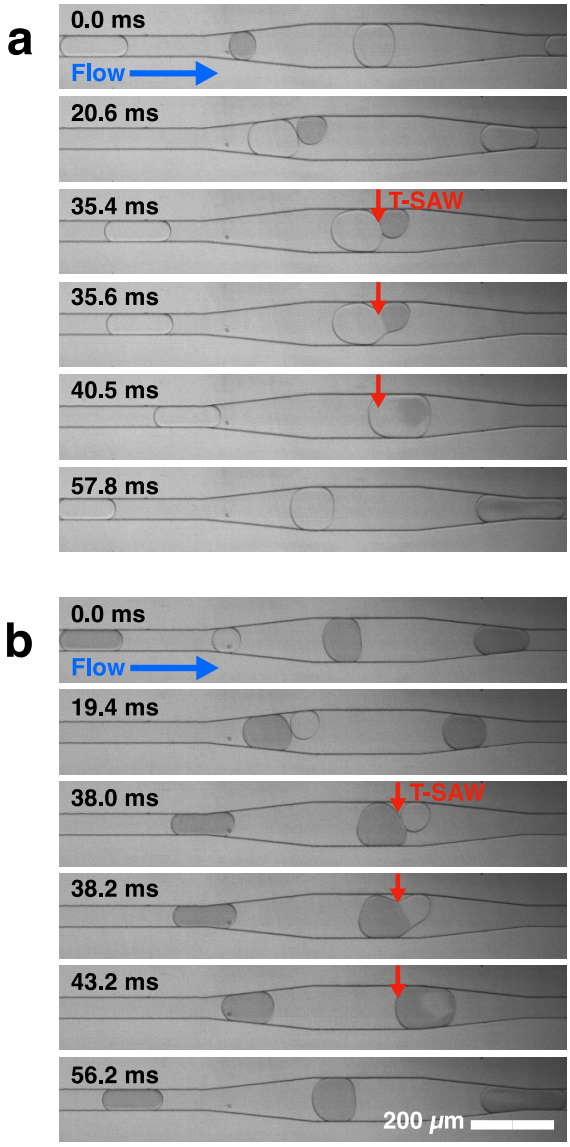

Figure 2. Time lapse imaging of 10Hz (a) front-triggered (FT) and (b) back-triggered (BT) merging. Flow direction is indicated by the blue arrows. Acoustic path is depicted by red arrows. In the absence of T-SAWs, no merging was observed (*SI Appendix*, Figure S2)

To characterize the effect of the acoustic path position relative to the position of targeted droplet pairs, we monitored the FT and BT droplet merging processes for different D values. By changing D, the position of droplet pairs within the merging chamber varies at the point of T-SAW actuation. For FT and BT

merging, efficiency E, given by the ratio of merged drops and number of intended merging events, decreases to both sides of central D values with a half-width time of ~10ms as shown in Figure 3a. The curve $E_{BT}(D)$ describing the dependence on D for BT merging is shifted to smaller delays compared with $E_{FT}(D)$ for FT merging, since the droplet pair has already proceeded further downstream in the merging region with reference to the position at which the laser detects the fluorescent drop. This curve displacement between FT and BT, $\Delta D = D_{FT} - D_{BT}$, can be estimated from the graph as the difference between delay values D_{FT} and D_{BT}, at which:

$$\int_0^{D_x} E(D)dD = \frac{1}{2}\int_0^{+\infty} E(D)dD$$

for FT and BT merging, respectively.

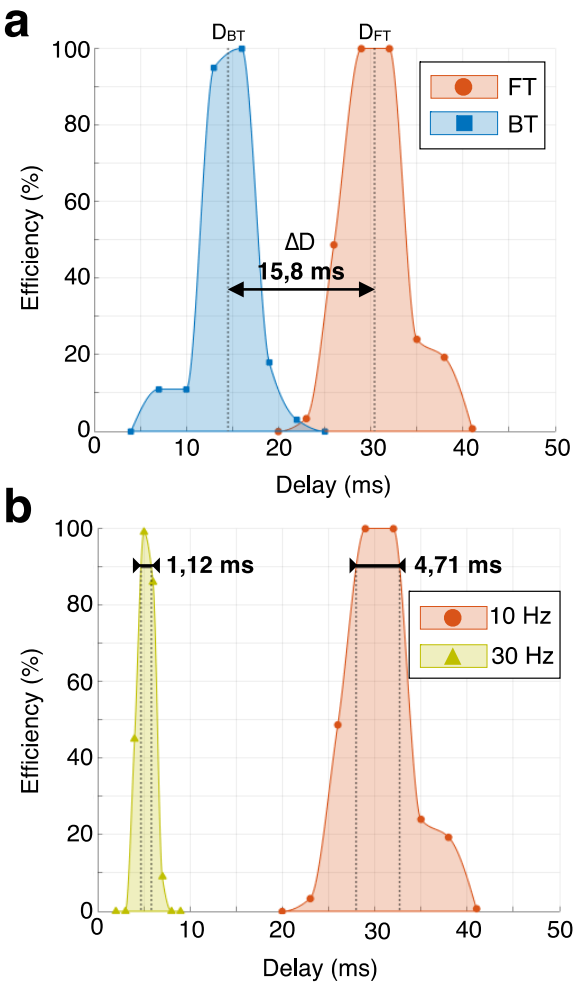

Figure 3. Distribution of merging efficiency as a function of delay time. (a) Comparison between FT and BT merging at a fixed fluorescein droplet frequency of 10 Hz. ΔD is depicted by the double ended arrow, while left and right dotted lines show D_{BT} and D_{FT}, respectively. (b) Comparison between 10 Hz and 30 Hz fluorescein droplet frequencies. Delay time intervals for highly efficient merging (≥ 90%) are represented by the span between dotted lines. T-IDT excitation frequency (162 MHz), duration (10 ms) and power (320 mW) were fixed during the experiment. Data were obtained by analyzing 100 droplet pairs per point.

The average delay shift between both curves ΔD = 15.8 ms after analyzing 1600 droplet pairs (Figure 3a). For comparison, we define the time taken (Δt_S) by the back droplet to reach the same position as the front droplet with reference to the location of the laser spot as $\Delta t_S = t_{SB} - t_{SF}$, with t_{SB} and t_{SF} being the back and front droplet screening times, respectively. For 10Hz fluorescein droplet production frequency we determine from 100 droplets that Δt_S =15.7 ± 0.3 ms (data not shown), which agrees with the value calculated for ΔD. While merging efficiency depends upon acoustic path positioning, our hybrid device can adapt to different droplet pair configurations and still achieve highly efficient merging.

The position of the acoustic path relative to the position of targeted droplet pairs is influenced by D and by droplet production frequency, as this latter affects droplet velocity. To understand how droplet production frequency and signal delay time impact droplet merging together, we measured merging efficiency at different combinations of production frequencies and delay times. Figure 3b shows FT merging efficiency at 10 Hz and 30 Hz fluorescein droplet production frequencies. We find that increasing the frequency of triggering droplets substantially reduces the D, as droplet pairs need less time to flow to the merging position. Higher droplet production frequency is also associated with a narrowing of the D range available to achieve high merging efficiency (≥ 90%), meaning that that precise timing becomes essential. The D range is reduced from 4.71 ms to 1.12 ms when fluorescein droplet frequency increases from 10 Hz to 30 Hz (Figure 3b). This reduction is explained by a decrease in interaction time between the acoustic path and droplets, due to an increased averaged droplet velocity from 15 µm ms^{-1} to 60 µm ms^{-1}. We found that higher merging efficiencies (≥ 90%) are achieved when the front edges of rear droplets are first hit by the acoustic path (Figure 2), regardless of whether the triggering droplet is in front or at the back of the pair.

Another important parameter influencing the acoustofluidic manipulation of droplets is the amount of acoustic momentum delivered to the system. To gain insight into how this influences merging efficiency, we observe merging efficiency as IDT excitation power is modulated. We performed FT and BT merging at three different fluorescein droplet frequencies (10 Hz, 20 Hz and 30 Hz). Our results suggest that merging efficiency critically depends on the power applied to the IDT (Figure 4). While no merging was observed at lower signal amplitudes, efficiency rapidly increases for FT and BT merging when signal power exceeds a critical level of 100 mW and 150 mW, respectively. This trend, forcing the comparison with a switched on/switched off phenomenon, is independent of the droplet frequencies considered within our experiments. Higher signal power is required for BT merging. This may be because datasets were acquired during two experiments, using two devices. Variations in the alignment of channels to T-IDTs may be responsible for the measured differences, as the amount of acoustic momentum damped by the PDMS in both devices may change slightly.[30]

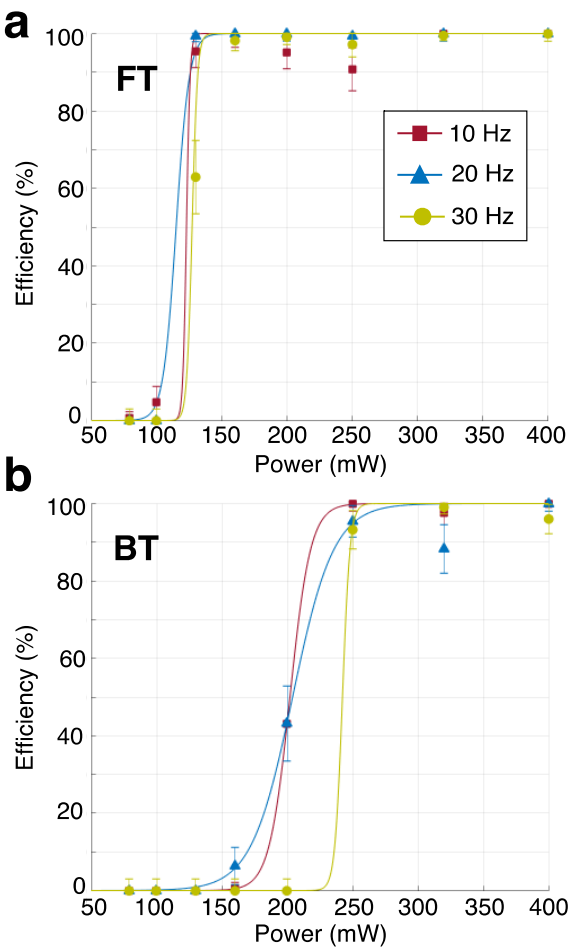

Figure 4. Merging efficiency depending on electric power used for (A) FT and (B) BT merging. T-IDT excitation signal frequency (162 MHz) and pulse duration (10 ms) were kept fixed during data acquisition. Curves were obtained by sigmoid fit using a Boltzmann equation. For each point, a total of 100 droplet pairs were analyzed. Errors were estimated for 95% confidence intervals.

Since the results shown in Figure 4 suggest that the amount of acoustic momentum transferred into the system affects merging efficiency, we quantified the influence of IDT excitation duration, here referred to as pulse duration (PD), on merging efficiency. Figure 5 shows merging efficiency for pulse durations at four different T-IDT excitation powers, ranging from 250 mW to 500 mW. The resulting curves, which show system behavior at the four different powers, all follow a similar trend and can be divided into three consecutive intervals: a rising, a plateau and a decreasing phase. The rising phase takes place in between 1 ms and 6 ms, as merging efficiency increases substantially for each power when the PD is incrementally increased. For a given PD, higher powers result in higher merging efficiency, as shown by the differences between 250 mW and 500 mW curves. Then in the second time range, between 6 ms and 20 ms PD, merging efficiency stabilizes and curves enter a plateau-like phase. After 20 ms, merging efficiency quickly drops.

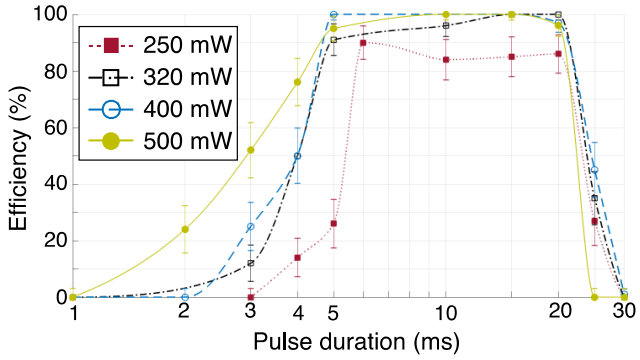

Figure 5. Distribution of merging efficiency as a function of pulse duration for different powers. IDT excitation signal frequency (162 MHz) and delay (29 ms) were kept fixed through the experiment. 150 droplet pairs were analyzed for each point. Errors were estimated for 95% confidence intervals.

DISCUSSION

The acoustofluidic device presented in this article allows for the merging of surfactant stabilized droplet pairs. Compared to other acoustic methods reported so far,[28] our device achieves selective merging as it is triggered following fluorescence screening of each droplet content. Furthermore, it exhibits a throughput of up to 10^5 droplet pairs merging per hour, with the ability to run continuously for more than 12 hours. By quantifying merging efficiency, we investigate the impact of IDT actuation delay, power and duration on the merging phenomenon. Our results show that the position of the acoustic path relative to the targeted droplet pair, together with the amplitude and duration of the T-SAW pulse, influences merging efficiency. Following each merging event, interfaces of the merged droplets rapidly form a bridge (< 200 µs) which relaxes to form a spherical drop minimizing its surface energy (*SI Appendix*, Figure S3).

As observed, merging successfully occurs when the acoustic pulse is actuated within a precise time window (Figure 3) of 4,71 ms and 1,12 ms for 10Hz and 30Hz FT merging. respectively. Since these time windows, when associated to droplets speed, correspond to a range of acoustic path positions relative to the position of the targeted droplet pair, our results are in agreement with previously reported work.[28] Nonetheless, while the other technique allows for the merging of droplets positioned 500 µm before and after the IDT, our device achieves droplets coalescence within a span of $\simeq$ 69 µm, only when the droplet pairs are in close vicinity of the T-IDT so that the acoustic path precisely hits the front of the rear drop. This difference between both devices, which allows us to perform localized and selective merging of single targeted droplet pairs without compromising sample compartmentalization in other droplets, can be attributed to channel design. The widening of the merging chamber in our device efficiently reduces pressure perturbations upstream and downstream of the acoustic path when compared to the use of a straight channel.

Once produced, the T-SAW pulse travels along the surface of the lithium niobate substrate before being refracted into the merging chamber fluid at a Rayleigh angle $\theta = arcsin(v_l/v_s)$, with v_l and v_s being the sound velocity in the liquid and on the substrate, respectively.[31] The resulting bulk waves are then attenuated, transferring momentum to the medium in form of

acoustic streaming, also termed microstreaming, as studied before in detail.[24–30] Since microstreaming velocity is considered proportional to the amplitude used to excite the T-SAWs pulse at the T-IDT,[34–36,38] we can infer from the results in Figure 4 that merging efficiency is dependent upon acoustic flow velocity. However, this brings forward the question: how acoustic streaming, which is an effect of the time averaged acoustic pressure field, could be responsible for surfactant stabilized coalescence of droplets?

Surfactant molecules are used to stabilize droplets and prevent coalescence due to steric repulsions of their tails at the interface between two droplets.[17] When two droplets get closer, the drainage of the liquid film separating them is responsible for an outward flow that leads to heterogenous distribution of the surfactant molecules along their surface. The resulting surface tension gradient leads to a stress, named Marangoni stress, which drives an inward flow counteracting film drainage, hence preventing coalescence of droplets.[39–41] As a T-SAW pulse is generated, the resulting microstreaming affects fluid flow in the vicinity of the acoustic path. We therefore hypothesize that acoustic streaming could disturb the Marangoni flow, permitting effective film drainage for droplet contact and merging. Moreover, when considering the on/off profile of the curves in Figure 4, we can further hypothesize the existence of a critical microstreaming velocity, above which the Marangoni flow would be sufficiently disturbed to allow merging. While changing surfactant concentration was reported to have no effect on T-SAWs merging efficiency[28], this possibility cannot be completely excluded given the low amount of data available on the subject. We expect that increasing surfactant concentration would increase the surface tension gradient responsible for the Marangoni flow. Consequently, if merging depends upon Marangoni flow disturbance, higher power might be required for efficient merging.

Another approach to explain the merging phenomenon observed within our device relies on a counterintuitive effect. It has been shown that when two droplets separate quickly, a pressure difference is created between their interiors and the bulk fluid, as viscous effects dominate.[42] This pressure difference may overcome surface tension, hence leading to the formation of two protrusions facing each other at droplets interface. If both protrusions reach a length higher than half the distance between the two droplets, contact is made and merging takes place.[14] In various simulations, the lengths of formed protrusions was associated with the acceleration of the front droplet relative to the rear droplet.[42,43] Such a phenomenon may be compatible with results obtained in Figure 4. In a horizontal plan, acoustic streamlines can be seen as two vortices, symmetric by the acoustic path center and rotating counter wise.[9,36,38] As a result, if the acoustic path is located at the interface between two droplets, the back droplet might be decelerated while the front one accelerates, thus leading to their separation at a speed influenced by acoustic streaming velocity. Therefore, we hypothesize that microstreaming velocity may influence droplet pairs separation, with a critical value above which the speed of protrusion formation together with their size enables droplets to contact and merge.

It should be noted that the merging phenomenon seems to be independent of the velocity of droplet pairs, as changes in droplet production frequency do not affect power threshold markedly for both FT and BT merging (Figure 4). However, this assumption must be taken carefully, as results reflect the phenomenon behavior at droplet velocities within the same order of magnitude. In the perspective of ultra-high throughput merging, drag force would be increased as it is proportional to speed of objects in laminar regime. Consequently, if merging relies on separation speed of droplets, a higher IDT input amplitude might be required to increase microstreaming velocity and reach the required separation conditions permitting merging of droplets.

It has been shown that as T-SAW pulse becomes longer, the transfer of momentum due to microstreaming is increased until it eventually reaches a plateau, defined by the acoustic pressure amplitude.[34,44] Therefore, the curve progression in Figure 5 suggests a merging efficiency directly proportional to the acoustic streaming velocity. The important point showed by this figure is the existence of an upper limit of pulse durations required to achieve effective merging within our device. For pulses lasting more than 20 ms, the substantial drop in merging efficiency can be explained by the fact that longer pulses affect the synchronization process of upcoming droplet pairs (*SI Appendix,* Figure S4).

In addition to the effect of microstreaming which results from the time averaged acoustic pressure field, a potential effect arising from the instantaneous acoustic field should also be considered. The 162 MHz AC signal used to excite the T-IDT during our experiments leads to the generation of millions of acoustic pressure maximums and minimums per second. These pressure oscillations, while travelling along the piezoelectric substrate, leak in the liquid under the form of bulk acoustic waves before hitting droplet interfaces. Consequently, we hypothesize that a mechanical effect associated with instantaneous acoustic field could lead to droplet interface vibration, at a frequency that could affect the surfactant layer. Indeed, such a vibrational effect has been theoretically studied[45,46] and observed[47,48] in experiments of droplet coalescence by the use of an AC electric field. In those studies, rapid changes of the electric field in kHz range promote dynamic instability in oil-water droplet interfaces, causing depletion of surfactant molecules, pore formation and merging.

To better understand if merging of surfactant stabilized droplets using T-SAWs is permitted by Marangoni flow disturbance, separation of droplets or/and by real time acoustic field pressure oscillations, future works should investigate the impact of surfactant concentration and liquid phases viscosities on merging efficiency as well as how acoustic pulses influence streaming outside and inside droplets. Additionally, velocities of all droplets involved in the merging process should be studied to validate the hypothesis of droplet separation-associated acoustic merging. This should be carried out together with an analysis of the effect of droplet diameters and deformation, since droplet compression has already been associated with merging of droplets.[14] Deformation of droplet interfaces was discussed previously in an article related to merging of surfactant stabilized droplets using T-SAWs.[28] In this work, the authors described an asymmetric deformation of the droplets caused by the acoustic streaming. We observed droplet deformations in our experiments and their role in acoustic merging is not to be excluded. The merging of surfactant stabilized droplets by T-SAWs at different frequencies in the MHz range has been briefly studied and found to have no influence on merging.[28] Nevertheless, our results call for a deeper study on how surfactant layers are affected under kHz, MHz and GHz acoustic fields, to better un-

derstand the potential impact of a vibrational effect on surfactant depletion, as mentioned for AC field electrocoalescence.[46–48]

CONCLUSION

Droplet-based fluidics has become a well-established and widely used technology, allowing rapid development in fields like high throughput single-cell sequencing and screening. Merging of droplets used as micro-containers is a key step in the workflow of many of these applications, for example, to add a drug to be tested[49] or barcodes in single-cell transcriptomics.[50] Here, we have introduced a versatile acoustic droplet merging technique that facilitates triggered merging of selected droplets at high speed using a fluorescence readout. The technology can be easily integrated with the many other acoustofluidic tools.[9,12,13,23] The ability to flexibly trigger merging, by either the front or the rear drop of the droplet pair, together with optimal synchronization and spacing of droplets, allows merging of only the desired droplet pairs, without influencing other drops in the channel.

In this work, highly specific and efficient merging was achieved within a narrow time window by means of triggered acoustic pulse actuation. The timing and position of the acoustic pulse was also precisely controlled relative to each detected droplet pair. Thus, we were able to ensure that the acoustic pulse initially contacted the target droplet pair at the front of the rear drop, and subsequently switched off before entry of the next droplet pair to the merging region. Our characterization of the dependency of merging efficiency on T-SAW power showed a sharp onset and the existence of a critical value, above which very high merging efficiency is achieved. The device attains a merging efficiency of 100% within the range of experimental parameters tested. In the absence of T-SAWs, no merging was ever detected, despite operating at a maximum merging frequency of 10^5 droplet pairs per hour – a 300-fold increase in throughput compared to previously reported acoustic merging techniques.[27,28] Following merging, rapid and complete mixing of droplet contents was also observed.

Future work should firstly be directed towards improving the detection strategy. For example, the implementation of real-time image analysis would enable live modulation of delay time and/or T-IDT excitation frequency, and thus, enhance system versatility. To finally realize ultra-high throughput merging in the kHz range, the method of droplet pairing should be revised, for example, by improving the microchannel design. Furthermore, comprehensively characterizing the influence of delay time and acoustic path width relative to the contact point of the acoustic pulse on the droplet interface would enable more rapid and efficient merging. To exploit the many advantages that acoustically driven micro total-analysis system bring over alternative methods, we aim to implement the existing system into other microfluidic workflows to achieve more complex tasks such as: drug screening, study of enzymes kinetics for directed evolution, and genetic and/or transcriptomic profiling of single cells.

ASSOCIATED CONTENT

Supporting Information

The Supporting Information is available free of charge on the ACS Publications website.

CAD design of PDMS mold with micrographs showing droplet production and spacing modules; Droplet motion through the merging chamber without T-SAWs; Speed of bridge formation and relaxation following merging; Droplets synchronization affected by long pulse duration. (PDF)

AUTHOR INFORMATION

Corresponding Authors

*E-mail : jean-christophe.baret@u-bordeaux.fr
*E-mail : Thomas.Franke@glasgow.ac.uk

Author Contributions

ΨThese authors contributed equally.

Notes

The authors declare no competing financial interest.

ACKNOWLEDGMENT

The authors would like to thank the European Commission for supporting this work through the Horizon 2020 Marie Sklodowska-Curie Action Innovative Training Network (ITN-EVOdrops). AV acknowledges the IdEx Bordeaux for the funding received in the framework ‘internationalisation of doctoral studies’. JCB acknowledges the support from the ‘Région Aquitaine’ and from the French Government ‘Investments for the Future’ Programme, University of Bordeaux Initiative of Excellence (IDEX Bordeaux) (Reference Agence Nationale de la Recherche (ANR)-10-IDEX-03-02).

REFERENCES

(1) Teh, S.-Y.; Lin, R.; Hung, L.-H.; Lee, A. P. Droplet Microfluidics. *Lab Chip* **2008**, *8* (2), 198–220. https://doi.org/10.1039/b715524g.

(2) Weitz, D. A. Perspective on Droplet-Based Single-Cell Sequencing. *Lab Chip* **2017**, *17* (15), 2539–2539. https://doi.org/10.1039/C7LC90069D.

(3) Agresti, J. J.; Antipov, E.; Abate, A. R.; Ahn, K.; Rowat, A. C.; Baret, J.-C.; Marquez, M.; Klibanov, A. M.; Griffiths, A. D.; Weitz, D. A. Ultrahigh-Throughput Screening in Drop-Based Microfluidics for Directed Evolution. *Proc. Natl. Acad. Sci. U. S. A.* **2010**, *107* (9), 4004–4009. https://doi.org/10.1073/pnas.0910781107.

(4) Pekin, D.; Skhiri, Y.; Baret, J.-C.; Le Corre, D.; Mazutis, L.; Ben Salem, C.; Millot, F.; El Harrak, A.; Hutchison, J. B.; Larson, J. W.; et al. Quantitative and Sensitive Detection of Rare Mutations Using Droplet-Based Microfluidics. *Lab Chip* **2011**, *11* (13), 2156–2166. https://doi.org/10.1039/c1lc20128j.

(5) Klein, A. M.; Mazutis, L.; Akartuna, I.; Tallapragada, N.; Veres, A.; Li, V.; Peshkin, L.; Weitz, D. A.; Kirschner, M. W. Droplet Barcoding for Single-Cell Transcriptomics Applied to Embryonic Stem Cells. *Cell* **2015**, *161* (5), 1187–1201. https://doi.org/10.1016/J.CELL.2015.04.044.

(6) Choi, S.-W.; Zhang, Y.; Xia, Y. Fabrication of Microbeads with a Controllable Hollow Interior and Porous Wall Using a Capillary Fluidic Device. *Adv. Funct. Mater.* **2009**, *19* (18), 2943–2949. https://doi.org/10.1002/adfm.200900763.

(7) Dupin, A.; Simmel, F. C. Signalling and Differentiation in Emulsion-Based Multi-Compartmentalized in Vitro Gene Circuits. *Nat. Chem.* **2019**, *11* (1), 32–39. https://doi.org/10.1038/s41557-018-0174-9.

(8) Beneyton, T.; Krafft, D.; Bednarz, C.; Kleineberg, C.; Woelfer, C.; Ivanov, I.; Vidaković-Koch, T.; Sundmacher, K.; Baret, J.-C. Out-of-Equilibrium Microcompartments for the Bottom-up Integration of Metabolic Functions. *Nat. Commun.* **2018**, *9* (1), 2391. https://doi.org/10.1038/s41467-018-04825-1.

(9) Schmid, L.; Weitz, D. A.; Franke, T. Sorting Drops and Cells with Acoustics: Acoustic Microfluidic Fluorescence-Activated Cell Sorter. *Lab Chip* **2014**, *14* (19), 3710–3718. https://doi.org/10.1039/c4lc00588k.

(10) Rambach, R. W.; Linder, K.; Heymann, M.; Franke, T. Droplet Trapping and Fast Acoustic Release in a Multi-Height Device with Steady-State Flow. *Lab Chip* **2017**, *17* (20), 3422–3430. https://doi.org/10.1039/C7LC00378A.

(11) Paik, P.; Pamula, V. K.; Fair, R. B. Rapid Droplet Mixers for Digital Microfluidic Systems. *Lab Chip* **2003**, *3* (4), 253–259. https://doi.org/10.1039/b307628h.

(12) Sesen, M.; Devendran, C.; Malikides, S.; Alan, T.; Neild, A. Surface Acoustic Wave Enabled Pipette on a Chip. *Lab Chip* **2017**, *17* (3), 438–447. https://doi.org/10.1039/C6LC01318J.

(13) Jung, J. H.; Destgeer, G.; Ha, B.; Park, J.; Sung, H. J. On-Demand Droplet Splitting Using Surface Acoustic Waves. *Lab Chip* **2016**, *16* (17), 3235–3243. https://doi.org/10.1039/C6LC00648E.

(14) Bremond, N.; Thiam, A. R.; Bibette, J. Decompressing Emulsion Droplets Favors Coalescence. *Phys. Rev. Lett.* **2008**, *100* (2), 1–4. https://doi.org/10.1103/PhysRevLett.100.024501.

(15) Niu, X.; Gulati, S.; Edel, J. B.; DeMello, A. J. Pillar-Induced Droplet Merging in Microfluidic Circuits. *Lab Chip* **2008**, *8* (11), 1837–1841. https://doi.org/10.1039/b813325e.

(16) Ahn, K.; Agresti, J.; Chong, H.; Marquez, M.; Weitz, D. A. Electrocoalescence of Drops Synchronized by Size-Dependent Flow in Microfluidic Channels. *Appl. Phys. Lett.* **2006**, *88* (26), 264105. https://doi.org/10.1063/1.2218058.

(17) Baret, J.-C. Surfactants in Droplet-Based Microfluidics. *Lab Chip* **2012**, *12* (3), 422–433. https://doi.org/10.1039/C1LC20582J.

(18) Thiam, A. R.; Bremond, N.; Bibette, J. Breaking of an Emulsion under an Ac Electric Field. *Phys. Rev. Lett.* **2009**, *102* (18), 188304. https://doi.org/10.1103/PhysRevLett.102.188304.

(19) Tan, W.-H.; Takeuchi, S. Timing Controllable Electrofusion Device for Aqueous Droplet-Based Microreactors. *Lab Chip* **2006**, *6* (6), 757–763. https://doi.org/10.1039/b517178d.

(20) Zagnoni, M.; Cooper, J. M. On-Chip Electrocoalescence of Microdroplets as a Function of Voltage, Frequency and Droplet Size. *Lab Chip* **2009**, *9* (18), 2652–2658. https://doi.org/10.1039/b906298j.

(21) Varma, V. B.; Ray, A.; Wang, Z. M.; Wang, Z. P.; Ramanujan, R. V. Droplet Merging on a Lab-on-a-Chip Platform by Uniform Magnetic Fields. *Sci. Rep.* **2016**, *6* (1), 37671. https://doi.org/10.1038/srep37671.

(22) Sun, J.; Wang, W.; He, F.; Chen, Z.-H.; Xie, R.; Ju, X.-J.; Liu, Z.; Chu, L.-Y. On-Chip Thermo-Triggered Coalescence of Controllable Pickering Emulsion Droplet Pairs. *RSC Adv.* **2016**, *6* (69), 64182–64192. https://doi.org/10.1039/C6RA12594H.

(23) Rambach, R. W.; Biswas, P.; Yadav, A.; Garstecki, P.; Franke, T. Fast Selective Trapping and Release of Picoliter Droplets in a 3D Microfluidic PDMS Multi-Trap System with Bubbles. *Analyst* **2018**, *143* (4), 843–849. https://doi.org/10.1039/C7AN01100H.

(24) Naseer, S. M.; Manbachi, A.; Samandari, M.; Walch, P.; Gao, Y.; Zhang, Y. S.; Davoudi, F.; Wang, W.; Abrinia, K.; Cooper, J. M.; et al. Surface Acoustic Waves Induced Micropatterning of Cells in Gelatin Methacryloyl (GelMA) Hydrogels. *Biofabrication* **2017**, *9* (1), 015020. https://doi.org/10.1088/1758-5090/aa585e.

(25) Chen, K.; Wu, M.; Guo, F.; Li, P.; Chan, C. Y.; Mao, Z.; Li, S.; Ren, L.; Zhang, R.; Huang, T. J. Rapid Formation of Size-Controllable Multicellular Spheroids: Via 3D Acoustic Tweezers. *Lab Chip* **2016**, *16* (14), 2636–2643. https://doi.org/10.1039/c6lc00444j.

(26) Alhasan, L.; Qi, A.; Al-abboodi, A.; Rezk, A.; Chan, P. P. Y.; Iliescu, C.; Yeo, L. Y. Rapid Enhancement of Cellular Spheroid Assembly by Acoustically Driven Microcentrifugation. **2016**, *2* (6), 1013–1022. https://doi.org/10.1021/acsbiomaterials.6b00144.

(27) Sesen, M.; Alan, T.; Neild, A. Microfluidic On-Demand Droplet Merging Using Surface Acoustic Waves. *Lab Chip* **2014**, *14* (17), 3325–3333. https://doi.org/10.1039/c4lc00456f.

(28) Sesen, M.; Fakhfouri, A.; Neild, A. Coalescence of Surfactant-Stabilised Adjacent Droplets Using Surface Acoustic Waves. *Anal. Chem.* **2019**, *91* (12), 7538–7545. https://doi.org/10.1021/acs.analchem.8b05456.

(29) Bourquin, Y.; Reboud, J.; Wilson, R.; Cooper, J. M. Tuneable Surface Acoustic Waves for Fluid and Particle Manipulations on Disposable Chips. *Lab Chip* **2010**, *10* (15), 1898–1901. https://doi.org/10.1039/c004506c.

(30) Rambach, R. W.; Skowronek, V.; Franke, T. Localization and Shaping of Surface Acoustic Waves Using PDMS Posts: Application for Particle Filtering and Washing. *RSC Adv.* **2014**, *4* (105), 60534–60542. https://doi.org/10.1039/C4RA13002B.

(31) Ding, X.; Li, P.; Lin, S.-C. S.; Stratton, Z. S.; Nama, N.; Guo, F.; Slotcavage, D.; Mao, X.; Shi, J.; Costanzo, F.; et al. Surface Acoustic Wave Microfluidics. *Lab Chip* **2013**, *13* (18), 3626–3649. https://doi.org/10.1039/c3lc50361e.

(32) Eckart, C. Vortices and Streams Caused by Sound Waves. *Phys. Rev.* **1948**, *73* (1), 68–76. https://doi.org/10.1103/PhysRev.73.68.

(33) Wiklund, M.; Green, R.; Ohlin, M. Acoustofluidics 14: Applications of Acoustic Streaming in Microfluidic Devices. *Lab Chip* **2012**, *12* (14), 2438–2451. https://doi.org/10.1039/c2lc40203c.

(34) Mitome, H. The Mechanism of Generation of Acoustic Streaming. *Electron. Commun. Japan (Part III Fundam. Electron. Sci.* **1998**, *81* (10), 1–8. https://doi.org/10.1002/(SICI)1520-6440(199810)81:10<1::AID-ECJC1>3.0.CO;2-9.

(35) Nowicki, A.; Secomski, W.; Wójcik, L. Acoustic Streaming: Comparison of Low-Amplitude Linear Model with Streaming Velocities Measured by 32-MHz Doppler. *Ultrasound Med. Biol.* **1997**, *23* (5), 783–791.

(36) Nowicki, A.; Kowalewski, T.; Secomski, W.; Wó, J. Estimation of Acoustical Streaming: Theoretical Model, Doppler Measurements and Optical Visualisation. *Eur. J. Ultrasound* **1998**, *7*, 73–81.

(37) Moudjed, B.; Botton, V.; Henry, D.; Ben-Hadid, H.; Garandet, J.-P.; Moudjed, B.; Botton, V.; Henry, D.; Hadid, H. Ben; Garandet, J.-P. Scaling and Dimensional Analysis of Acoustic Streaming Jets. *Phys. Fluids* **2014**, *26*, 093602. https://doi.org/10.1063/1.4895518ï.

(38) Alghane, M.; Chen, B. X.; Fu, Y. Q.; Li, Y.; Luo, J. K.; Walton, A. J. Experimental and Numerical Investigation of Acoustic Streaming Excited by Using a Surface Acoustic Wave Device on a 128° YX-LiNbO3 Substrate. *J. Micromechanics Microengineering* **2011**, *21* (1), 015005. https://doi.org/10.1088/0960-1317/21/1/015005.

(39) Baret, J. C.; Kleinschmidt, F.; Harrak, A. El; Griffiths, A. D. Kinetic Aspects of Emulsion Stabilization by Surfactants: A Microfluidic Analysis. *Langmuir* **2009**, *25* (11), 6088–6093. https://doi.org/10.1021/la9000472.

(40) Chan, D. Y. C.; Klaseboer, E.; Manica, R. Film Drainage and Coalescence between Deformable Drops and Bubbles. *Soft Matter* **2011**, *7* (6), 2235–2264. https://doi.org/10.1039/c0sm00812e.

(41) Jones, A. F.; Wilson, S. D. R. The Film Drainage Problem in Droplet Coalescence. *J. Fluid Mech.* **1978**, *87* (2), 263–288. https://doi.org/10.1017/S0022112078001585.

(42) Lai, A.; Bremond, N.; Stone, H. A. Separation-Driven Coalescence of Droplets: An Analytical Criterion for the Approach to Contact. *J. Fluid Mech.* **2009**, *632*, 97–107. https://doi.org/10.1017/S0022112009007320.

(43) Yoon, Y.; Baldessari, F.; Ceniceros, H. D.; Leal, L. G. Coalescence of Two Equal-Sized Deformable Drops in an Axisymmetric Flow. *Phys. Fluids* **2007**, *19* (10), 102102. https://doi.org/10.1063/1.2772900.

(44) Mitome, H.; Kozuka, T.; Tuziuti, T. Measurement of the Establishment Process of Acoustic Streaming Using Laser Doppler Velocimetry. *Ultrasonics* **1996**, *34* (2–5), 527–530. https://doi.org/10.1016/0041-624X(95)00063-9.

(45) Brown, A. H.; Hanson, C. Effect of Oscillating Electric Fields on Coalescence in Liquid+liquid Systems. *Trans. Faraday Soc.* **1965**, *61*, 1754–1760. https://doi.org/10.1039/tf9656101754.

(46) Eow, J. S.; Ghadiri, M.; Sharif, A. O.; Williams, T. J. Electrostatic Enhancement of Coalescence of Water Droplets in Oil: A Review of the Current Understanding. *Chem. Eng. J.* **2001**, *84*, 173–192. https://doi.org/10.1016/S1385-8947(00)00386-7.

(47) Manica, R.; Connor, J. N.; Clasohm, L. Y.; Carnie, S. L.; Horn, R. G.; Chan, D. Y. C. Transient Responses of a Wetting Film to Mechanical and Electrical Perturbations. *Langmuir* **2008**, *24* (4), 1381–1390. https://doi.org/10.1021/la701562q.

(48) Priest, C.; Herminghaus, S.; Seemann, R. Controlled Electrocoalescence in Microfluidics: Targeting a Single Lamella. *Appl. Phys. Lett.* **2006**, *89* (13), 2004–2007.

https://doi.org/10.1063/1.2357039.
(49) Brouzes, E.; Medkova, M.; Savenelli, N.; Marran, D.; Twardowski, M.; Hutchison, J. B.; Rothberg, J. M.; Link, D. R.; Perrimon, N.; Samuels, M. L. Droplet Microfluidic Technology for Single-Cell High-Throughput Screening. *Proc. Natl. Acad. Sci. U. S. A.* **2009**, *106* (34), 14195–14200. https://doi.org/10.1073/pnas.0903542106.
(50) Rotem, A.; Ram, O.; Shoresh, N.; Sperling, R. A.; Goren, A.; Weitz, D. A.; Bernstein, B. E. Single-Cell ChIP-Seq Reveals Cell Subpopulations Defined by Chromatin State. *Nat. Biotechnol.* **2015**, *33* (11), 1165–1172. https://doi.org/10.1038/nbt.3383.

For Table of Contents Only